International Journal of Greenhouse Gas Control 151 (2026) 104589

Contents lists available at ScienceDirect

International Journal of Greenhouse Gas Control

journal homepage: www.elsevier.com/locate/ijggc

pH-equilibrated ocean alkalinization: Mesoscale evaluation of long-term stability

Samira Jamali Alamooti [a], Federico Comazzi [b], Eleonora Kratter Thaler [a], Sara Groppelli [c], Davide Calvi [c], Guido Raos [a,*], Piero Macchi [a,*]

[a] Department of Chemistry, Materials and Chemical Engineering, Politecnico di Milano, via Mancinelli 7, 20131 Milano, Italy
[b] Limenet®, Via Giovanni Amendola 4-6, 23900 Lecco, Italy
[c] Department of Earth and Environmental Science, University of Milano Bicocca, Piazza della Scienza 1 e 4, 20126, Milano Italy

ARTICLE INFO

Keywords:
Seawater alkalinization
CO_2 storage
Marine carbonate chemistry
Climate change mitigation
Bicarbonate stability

ABSTRACT

A new pH-equilibrated ocean alkalinization method was evaluated at the mesoscale level to assess the long-term stability of carbon retained as bicarbonate in seawater. Natural seawater was enriched in bicarbonate by reacting $Ca(OH)_2$ with CO_2 in natural seawater, adjusted to match ambient pH, and introduced into controlled mesocosms to increase the Dissolved Inorganic Carbon (DIC) content by 250 to 1990 μmol C/L above natural levels. The stability of chemical parameters in the mesocosms was monitored over a 76-day period. Under moderate alkalinization ($\leq$1000 μmol C/L of added DIC), >90% of the added inorganic carbon remained stable for nearly two months. In contrast, treatments leading to an aragonite saturation state (Ω_{Ar}) exceeding 10, exhibited rapid declines in stability due to secondary carbonate precipitation and CO_2 degassing, particularly at high temperatures. While natural seawater salinity and pH did not directly induce instability, they modulated the carbonate saturation state and therefore they must be considered for a correct prediction of the system behavior. Seasonal fluctuations in seawater characteristics, namely salinity, temperature, and pH, were found to influence theoretical Ω_{Ar} and should be considered for alkalinity dosing and site selection. These findings underscore the importance of assessing real-time, site-specific conditions for effective and safe implementation.

1. Introduction

According to the United Nations Framework Convention on Climate Change; UNFCCC Paris Agreement, limiting global warming below 2 °C relative to pre-industrial levels, requires substantial reductions of CO_2 and other greenhouse gases emissions (Intergovernmental Panel on Climate Change (IPCC), 2023). Carbon capture and storage (CCS) and negative emission technologies represent important complementary approaches to achieve those targets. However, most relevant technologies, like ocean-based CCS strategies,(National Academies of Sciences, 2022; Vibbert and Park, 2022) are not yet ready for large scale application.

The oceans have absorbed approximately 25 % of the anthropogenic CO_2, leading to seawater acidification (Köhler, 2020; Renforth et al., 2022; Zhuang et al., 2023). CO_2 is in equilibrium with carbonic acid and its conjugate bases in seawater (Capelle et al., 2020; Zeebe and Wolf-Gladrow, 2001):

$$CO_2(aq) + H_2O(l) \rightleftharpoons HCO_3^-(aq) + H^+(aq) \rightleftharpoons CO_3^{2-}(aq) + 2H^+(aq) \quad (1)$$

Consequently, the seawater pH decreased from 8.2 in preindustrial times to 8.1 currently. Dissolution of carbonate minerals shifts equilibrium (1) toward (bi)carbonate ions, implying permanent CO_2 storage without ocean acidification. This ocean alkalinity enhancement (OAE) is a method studied for over 20 years (Hartmann et al., 2013; Ilyina et al., 2013; Intergovernmental Panel on Climate Change (IPCC), 2005; Kheshgi, 1995; Renforth et al., 2022; Ringham et al., 2024; Taylor et al., 2016).

OAE can be accelerated by introducing calcium carbonate minerals featuring high reactive surface areas (Caldeira and Rau, 2000; Kirchner et al., 2020b; Rau, 2011; Rau and Caldeira, 1999) with seawater and CO_2 into a reactor (Chou et al., 2015; Kirchner et al., 2020a):

$$CO_2(aq) + CaCO_3(s) + H_2O(1) \rightleftharpoons Ca^{2+}(aq) + 2HCO_3^-(aq) \quad (2)$$

This approach, called Accelerated Weathering of Limestone (AWL), does not rely on deep-sea release, but requires high amounts of water

* Corresponding authors.
E-mail addresses: guido.raos@polimi.it (G. Raos), piero.macchi@polimi.it (P. Macchi).

https://doi.org/10.1016/j.ijggc.2026.104589
Received 2 September 2025; Received in revised form 29 November 2025; Accepted 23 January 2026
Available online 29 January 2026

and large reactors. In the case of an incomplete reaction, CO_2 degassing and seawater acidification occur (Huysmans et al., 2025). Afterwards, a Buffered-AWL (BAWL) method (Campo et al., 2021; Caserini et al., 2021; De Marco et al., 2023) was proposed: $Ca(OH)_2$ is added to buffer the unreacted CO_2 and produce a bicarbonate-rich solution at the same pH of seawater:

$$2CO_2(aq) + Ca(OH)_2(s) + H_2O(1) \rightleftharpoons Ca^{2+}(aq) + 2HCO_3^-(aq) \quad (3)$$

This allows permanent CO_2 storage, without seawater acidification and CO_2 degassing (De Marco et al., 2023; Varliero, 2021). Cost analysis of BAWL (De Marco et al., 2023) and mass and energy balance studies (Campo et al., 2021; Caserini et al., 2021) revealed that the deeper is the discharge point, the lower is $Ca(OH)_2$, and consequently, the energy and CO_2 emission for $Ca(OH)_2$ production, while the pipeline costs increase.

An improvement of BAWL based solely on $Ca(OH)_2$ addition to a mixture of CO_2 and seawater was eventually proposed: the near-pH-equilibrated ocean alkalinization (Varliero et al., 2024). A series of experimental reactors were designed and constructed to produce the bicarbonate-enriched solution at the seawater pH. The aim was to upgrade the technique from the laboratory phase to a realistic field implementation and to evaluate its sustainability. From a geochemical perspective, the sustainability depends on the amount of the formed carbonate and the stability of seawater alkalinity, avoiding secondary carbonate precipitation and CO_2 release (Bach et al., 2019; Hartmann et al., 2023).

At laboratory scale, the threshold saturation state of aragonite, Ω_{Ar}, that prevents mineral precipitation was determined (Varliero et al., 2024). Ω_{Ar} is defined as (Moras et al., 2022; Zeebe and Wolf-Gladrow, 2001):

$$\Omega_{Ar} = \frac{[Ca^{2+}][CO_3^{2-}]}{K_{SP}} \quad (4)$$

with K_{SP} being the solubility product of aragonite.

A pilot plant installed in the harbor of La Spezia, Italy (Varliero et al., 2024), produced the near-pH-equilibrated bicarbonate-enriched solution was injected into natural seawater. Laboratory tests assessed the chemical stability of the absorbed carbon. A total carbon concentration below 1000–1500 μmol/L was considered safe for long-term stability of the solution. The broad threshold range accounts for the variability of the seawater and environmental conditions.

To scale up the approach, mesocosm experiments were later conducted within a controlled greenhouse environment. Mesocosms are outdoor, semi-controlled ecosystems, including experimental ponds and streams, where physical dimensions and fundamental water chemistry are regulated. Each mesocosm contains a few cubic meters of seawater, making it larger than a microcosm but smaller than a full-scale ecosystem (Boyle and Fairchild, 1997).

Biological studies in mesocosms have shown that planktonic communities can exhibit a high degree of resilience to OAE in oligotrophic environments (Bach et al., 2019; Sánchez et al., 2024; Xin et al., 2024). In our project, biological monitoring was integrated alongside chemical monitoring to comprehensively evaluate the process impact on marine microorganisms (Groppelli et al., 2026). This article focuses exclusively on the carbonate chemistry, the efficiency of near-pH-equilibrated OAE, and the long-term stability of CO_2 stored in seawater.

2. Experimental section

2.1. Pilot scale experiment

The near-pH-equilibrated bicarbonate-enriched solutions were prepared using natural seawater collected at Porto Mirabello (44°06′04.7″N, 9°49′40.6″E) in La Spezia (northern Tyrrhenian Sea, Italy), at a depth of ca. 2 m using a draft pump with a flow rate of 25 L/s. This seawater was first mixed with 100 % gaseous CO_2 supplied by Linde Gas Italia S.r.l.. The resulting acidic output stream was then transferred to a second mixing stage, where a slurry of $Ca(OH)_2$ was added, ensuring that the pH of the solution matched the starting pH of the natural seawater. The pH control strategy of the pilot plant was designed so that the outlet pH matched the real-time pH of the incoming seawater. To achieve this, the hydroxide dosing pump was continuously regulated by comparing inlet and outlet pH signals. In practice, small departures from the target value (typically up to 0.3 – 0.35 pH units) may occur due to the intrinsic response time and inertia of the control loop, as well as the measurement uncertainty associated with seawater pH measurement. While the current system provides sufficient precision for the objectives of this study, an optimized industrial implementation, beyond the scope of this work, could employ a higher-accuracy pH control strategy to achieve tighter control.

The $Ca(OH)_2$ slurry was prepared by mixing seawater with $Ca(OH)_2$ powder (supplied by Unicalce S.p.a.) in a weight ratio of 30:1. The incoming seawater turbidity was continuously monitored using a TurbSense SN—TSIR—9667 probe, and the pH of the output stream was regulated with a pHSense 5–381 probe to ensure process consistency.

To evaluate the long-term stability of bicarbonate in natural seawater, an experiment was conducted at the La Spezia location from March 14 till May 29, 2024, for 76 days in total. The experimental design included five distinct treatments, each replicated three times, across 15 land-based mesocosms. To minimize external environmental influences, the mesocosms were randomly placed under a transparent cover. Groups of three mesocosms were each enclosed by a containment pool filled with water, serving as a buffer against temperature fluctuations. Each mesocosm consisted of a transparent low-density polyethylene bag with a volume of 1000 liters. The mesocosms were filled with natural seawater mixed with different concentrations of the bicarbonate-enriched solution. Physicochemical parameters were monitored with weekly sampling until day 27, and biweekly thereafter.

Table 1 summarizes the parameters employed for each treatment, ranging from untreated seawater (used as the control mesocosms) to seawater highly supersaturated with respect to aragonite (to simulate a condition well above the threshold limit). The theoretical Ω_{Ar} was calculated using CO2SYS Excel Macro (version 2.5) (Pierrot et al., 2006), based on the properties of natural seawater reported at the end of 2023, which had a practical salinity of 38.3 at temperature of 19.8 °C, a pH of 8, a Total Alkalinity (TA) of 2602 μeq/L, and a Dissolved Inorganic Carbon (DIC) of 2562 μmol C/L.

2.2. Measurements

Considering the governing equations and variables, the marine carbonate chemistry is fully determined by knowing at least two out of three variables (DIC, TA, or pH). Along with hydrographic conditions, such as salinity and temperature, the entire system can be fully characterized. In this study, TA, DIC, pH, and conductivity were systematically measured, and the precipitates were analyzed by X-ray diffraction

Table 1
The parameters used for each of the 5 treatments tested in the mesocosms.

ID	Treatments	Treated volume (L)	Total mesocosm volume (L)	Added DIC (μmol C/L)	Theoretical Ω_{Ar}
C	Control seawater	0	1000	0	3.4
L	Low concentration	33	1000	250	3.9
M	Medium concentration	67	1000	508	4.3
H	High concentration	133	1000	1008	5.2
S	Supersaturated state	263	1000	1992	7.1

(XRD). All measurements were carried out in the laboratories of the Polytechnic University of Milan. DIC and TA serve as indicators of CO_2 release and carbonate precipitation. Specifically, the precipitation of calcium carbonate decreases DIC and TA in a 1:2 ratio, whereas CO_2 release without precipitation results in a reduction of DIC while TA remains unchanged (Zeebe and Wolf-Gladrow, 2001).

The pH was measured using a MATTLER TOLEDO Seven Excellence S475 multiparameter instrument equipped with an InLab Routine Pro-ISM pH electrode, with probe calibration performed biweekly based on the National Institute of Standards and Technology (NIST) scale, employing certified buffer solutions with pH values of 4.01, 7.00, and 10.00. According to the manufacturer specifications, the instrument provides a pH accuracy of ±0.002 pH units and a resolution of 0.001 pH units. Conductivity was also measured with a METTLER TOLEDO Seven Excellence S475, calibrated biweekly using a standard solution of 12,880 μS/cm as the reference. The instrument accuracy is ±0.5 % of the reading, with a resolution between 0.001 and 2 μS/cm, depending on the range. Each treatment was run in triplicate mesocosms ($n = 3$), and the error bars in all figures represent the standard deviation among the three independent mesocosms.

For all carbonate system calculations (like the computation of Ω_{Ar}), the pH values measured on the NIST scale were not used directly. Instead, they were converted to the seawater scale using the empirical model of Badocco et al. (2021), which expresses seawater scale pH as a function of pH measured on the NIST scale, temperature, and salinity. Badocco and co-workers (Badocco et al., 2021) reported an overall uncertainty of 0.009 – 0.016 pH units for the converted seawater scale pH. Accordingly, we consider ±0.02 pH units as a conservative estimate of the uncertainty associated with the pH values used in our carbonate system analysis.

TA was quantified using an automated titration system (Hanna Instruments HI84531) operated in low-range mode (30- 400 mg $CaCO_3$/L). Calibration of the acid pump was performed before each analysis session. The integrated pH electrode was calibrated biweekly using buffer solutions at pH values of 4.01, 7.01, and 8.30. According to the instrument specifications, the resolution is 0.1 mg $CaCO_3$/L, and the accuracy in low-range mode is ±1 mg $CaCO_3$/L or ±3 % of the reading (whichever is greater) at 25 °C. TA values were converted to μeq/L for consistency with carbonate chemistry conventions.

For TA, pH, and conductivity, each sample was measured once; therefore, the error bars shown in Figures represent the standard deviation among the three replicate mesocosms for each treatment.

DIC was determined through acidification followed by non-dispersive infrared absorbance using an Analytik Jena multi-NC 2100S analyzer. Each sample was automatically measured three times, and the reported value corresponds to the mean of these measurements. According to the manufacturer specifications, the repeatability of the instrument measurement is CV = 1–2 %. If the coefficient of variation exceeded 2 %, the system performed a fourth measurement and automatically discarded the outlier. Instrument blanks were performed using deionized water at the beginning and end of each analytical session, and calibration was verified daily using a 2500 μmol C/L standard solution.

The temperature of the samples in the laboratory was measured using the integrated temperature sensor of the SevenExcellence pH electrode, which provides a resolution of 0.1 °C and an accuracy of ±0.1 °C. The temperature and light intensity of the mesocosms were measured using the HOBO Pendant MX Temperature/Light Data Loggers, placing one sensor for each pool. The sensor characteristics are a temperature accuracy of ±0.5 °C and a light accuracy typical for direct sunlight of ±10 %. Temperature measurements were recorded every five minutes. This study considers the average temperature of all five pools.

CO2SYS (Pierrot et al., 2006) was employed to calculate all other variables, particularly Ω_{Ar}, using DIC and pH, with the pH converted to the seawater scale (Badocco et al., 2021) along with temperature and practical salinity derived from the measured conductivity (Lewis, 1980). The calculations utilized carbonate system constants from Mehrbach (Mehrbach et al., 1973) refit by Dickson and Millero (Dickson and Millero, 1987) with supplementary constants from Dickson (Dickson, 1990) for $KHSO_4$, and from Uppström (Uppstrom, 1974) for total borate concentration. The calculated Ω_{Ar} values were further corrected to account for the effects of calcium ion variation due to $Ca(OH)_2$ dissolution and $CaCO_3$ precipitation, as described by Moras et al. (Moras et al., 2022).

The process efficiency ($\eta_{process}$) is defined as the ratio between the observed increase of carbon content in treated seawater at the time of discharge and the theoretical maximum increase expected from the amount of CO_2 inflated through the process described in Eq. (3). $\eta_{process}$ depends on phenomena that may occur in the reactor or between the reactor and the delivery point, which may reduce the carbon effectively dissolved in seawater. Therefore, $\eta_{process}$ inherently captures any incomplete CO_2 dissolution, gas-liquid mixing inefficiency, degassing, or losses occurring during transport or at discharge point(Varliero et al., 2024).

$$\eta_{process} = \frac{DIC(0) - DIC_{sw}(0)}{\Delta_{DIC}} \tag{5}$$

where DIC(0) and $DIC_{SW}(0)$ are the initial DIC values, measured on the first day on the treated and control seawater, respectively, and Δ_{DIC} is the expected increase in DIC based on the injected CO_2.

On the other hand, the stability efficiency ($\eta_{St}(t)$) reflects the temporal stability of the treatment under experimental conditions. It is defined as the time-dependent ratio of the difference in DIC between the treated and control seawater at a specific time t [DIC(t) and $DIC_{SW}(t)$, respectively], to the same difference measured on the first day (Varliero et al., 2024):

$$\eta_{St}(t) = \frac{1}{r(t)} \times \frac{DIC(t) - DIC_{sw}(t)}{DIC(0) - DIC_{sw}(0)} \tag{6}$$

where:

$$r(t) = \frac{DIC_{sw}(t)}{DIC_{sw}(0)} \tag{7}$$

Here $r(t)$ represents the relative change in DIC of control seawater over time, capturing baseline variations due to environmental and experimental conditions, for example due to water evaporation. Since DIC responds to both runaway precipitation and CO_2 degassing, it provides the best indicator to assess the stability of the system over time. Because $\eta_{St}(t)$ relies solely on experimentally measured DIC values, it is a fully empirical metric and does not involve any theoretical or stoichiometric assumptions.

Precipitates were collected from each mesocosm at the end of the experiment. The solid samples were separated through filtration. Due to the features of the experimental setup, it was not possible to perform a quantitative collection of the precipitates. Powder X-ray diffraction was carried out on a Bruker D2-phaser diffractometer, using Cu-Kα radiation, with X-ray generator working at 30 kV and 10 mA. The XRD patterns were collected in the range 2θ = 10–60 °, with step-size of 0.006° and time per step 0.4–1.0 s depending on the scattering power of the sample. The software QualX 2.0 (Altomare et al., 2015) was used for the phase identification and Topas academic v6 (Coelho, 2018) for quantifying the composition. In the refinements, unit cell parameters and atom positions of calcite, aragonite, halite, quartz and gypsum were fixed at the known values at ambient conditions and only the scale parameter of each phase was refined, together with the crystallite size parameters and a preferred orientation parameter for gypsum and halite, both strongly affected. It was also necessary a refinement of the unit cell parameters for the Mg rich calcite structure, given that the Mg content in the solid forms we identified significantly deviates from that of the known structure (Falini et al., 1998).

3. Results and discussion

The aim of this study, following the previous determination of the safe limit of CO_2 storage in seawater as bicarbonate (Varliero et al., 2024), was the scalability of the process at the mesoscale and the assessment of the process efficiency and the safe limits. This included examining the efficiency of the near-pH-equilibrated ocean alkalinization process and evaluating its long-term stability to mitigate risks such as secondary precipitation, CO_2 degassing, and pH inconsistencies, particularly when the saturation state of the treated seawater approaches the critical threshold.

Treatments included four concentrations of added DIC: Low (250 μmol C/L), Medium (508 μmol C/L), High (1008 μmol C/L), and Supersaturated (1992 μmol C/L). Three mesocosms were assigned for each treatment. Additionally, three mesocosms containing only natural seawater served as experimental baselines. The selection of DIC addition levels was informed by our previous laboratory-scale assessment of the near-pH-equilibrated process (Varliero et al., 2024), where we identified that aragonite precipitation begins once total DIC approaches the upper stability limit of seawater. For the mesoscale experiment, we therefore chose a range of added DIC concentrations spanning: values well below the previously identified precipitation threshold, a level close to the maximum stable range, and a higher level expected to exceed the threshold. This design allowed us to evaluate both stable and unstable regimes and to confirm the onset of precipitation under supersaturated conditions.

Fig. 1 reports the pH for each mesocosm along with sample temperatures recorded during laboratory measurements. All pH values shown in this figure are reported on the NIST scale, consistent with the electrode calibration procedure. The pH for the M and S treatments slightly exceeded the expected values, possibly due to limitations in the reactor's ability to precisely regulate the output stream pH, especially for high concentrations of bicarbonate. Additionally, the sample temperature during laboratory analysis on day 19 artificially increased the pH measured on that day for all treatments. Apart from that, a clear trend of pH decrease is evident for the S treatment, as well as, with a slight delay, for the H treatment. This suggests a loss of alkalinity due to the secondary precipitation and consequent CO_2 degassing. In contrast, the L treatment exhibits a stable pH trend, mirroring the Control mesocosm.

Fig. 2 reports the conductivity (normalized to 25 °C), primarily governed by the concentration and diffusivity of dissolved ionic species, which is directly related to salinity and temperature. In principle, the conductivity of the treatments was expected to increase progressively from the C to the S treatment. However, as shown in Fig. 2, the S and H treatments do not exhibit the highest conductivity, which is again a clue of an incipient loss of ions at the beginning of the process due to association of the ions and ultimately to precipitation reactions. In contrast, C, L, and M treatments follow the expected conductivity trend, increasing proportionally with the added ionic species and being influenced by sample temperature variations during measurement, like for the pH data.

In Fig. 3, DIC and TA are reported as a function of time for each treatment, together with average temperature of pools monitored on-site over time. S and H treatments exhibited a sharp decline in both TA and DIC immediately after the experiment began, indicating significant instability from the outset. This phenomenon can be attributed to

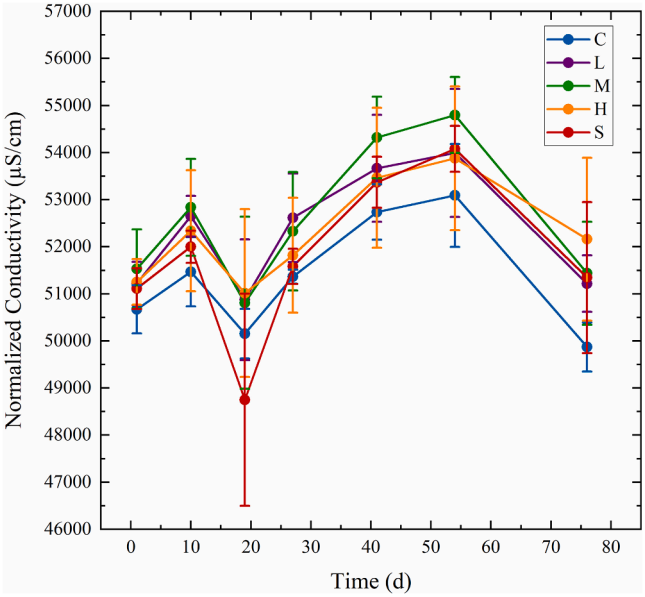

Fig. 2. Average conductivity normalized to 25 °C. Conductivity refers to electrical conductivity (μS/cm). Error bars represent standard deviation across replicate mesocosms.

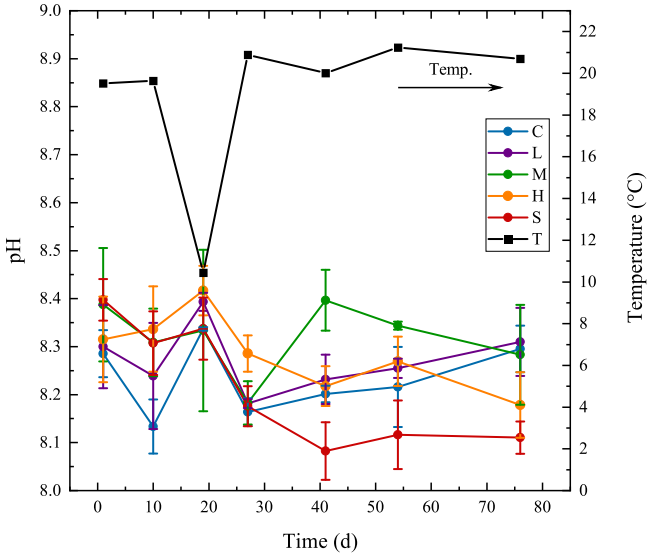

Fig. 1. Average pH (reported on the NIST scale) measured for each treatment over time, and average sample temperature. Error bars represent standard deviation across replicate mesocosms. Error bars represent standard deviation across replicate mesocosms.

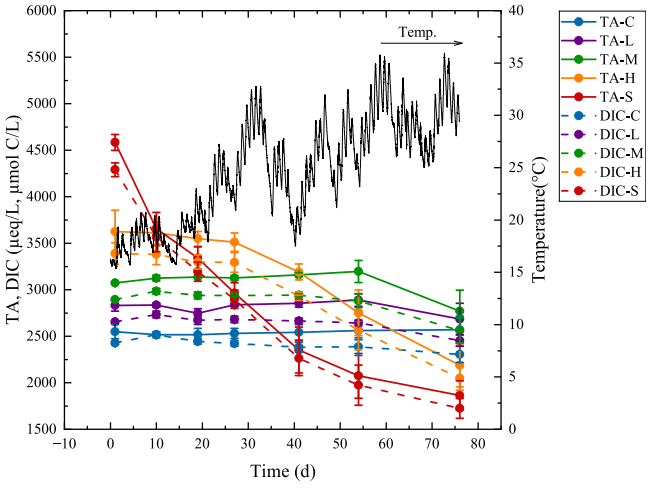

Fig. 3. Average TA, DIC for each treatment, and average temperature of pools monitored on-site over time. Error bars represent standard deviation across replicate mesocosms.
TA (total alkalinity) and DIC (dissolved inorganic carbon) are expressed in µeq/L and µmol C/L, respectively.

the fact that natural seawater is already supersaturated with respect to aragonite (see the Ω_{Ar} values in Table 1). The excessive alkalinity addition led to a further increase of the supersaturation state and promoting the nucleation and eventually the precipitation of solid carbonates. Consequently, this resulted in a loss of total alkalinity in solution. Because the carbonates are naturally supersaturated, once the nucleation and precipitation are triggered the amount of solid formed may well exceed the injected alkalinity. This is evident in the S and H treatments, where alkalinity fell below that of the control treatment by days 40 and 76, respectively.

In contrast, L and M treatments, with lower added alkalinity, exhibited relative stability up to day 55 of the experiment, with TA and DIC trends closely matching those of the control treatment. However, beyond day 55, as the temperature within the greenhouse hosting the mesocosms rose and occasionally overcame 35 °C, both parameters gradually declined in these treatments as well. This can be attributed to the reduced solubility of both carbonate minerals and gaseous CO_2 at higher temperatures. This suggests that a temperature threshold must also be considered, above which near-pH-equilibrated alkalinization is not efficient, particularly at very high Ω_{Ar} levels. Analysis of the relative declines in TA and DIC shows that their ratio is approximately 1:1, indicating that the observed instability results from a combination of secondary carbonate precipitation and CO_2 degassing.

It is important to note that the magnitude of these TA and DIC declines (tens to hundreds of μeq/L and μmol C/L, respectively) is far greater than the analytical uncertainty of the measurements (refer to measurements section), ensuring that the identification of instability driven by extensive carbonate precipitation is not limited by instrumental precision.

In Fig. 1, the pH of the seawater samples was measured in the laboratory at a nearly constant temperature of 20 °C. In contrast, Fig. 3 shows the on-site seawater temperature across the pools which fluctuated significantly due to spring conditions affecting the mesocosms during the latter half of the experiment.

The calculated process efficiency for all treatments exceeds 90 %, ranging from 90.5 % to 95.4 % (Figure S1, Supporting Information). This value was obtained by comparing the observed DIC increase after preparation with the theoretical maximum increase expected from the injected CO_2. This is significantly higher than the average efficiency of approximately 80 % observed in the pilot plant launched in 2022 (Varliero et al., 2024). As mentioned in the previous section, the process efficiency is influenced by factors such as the reactor design, the control of operational parameters, and the potential pitfalls in the delivery pathway. Therefore, minimizing these limitations will lead to a further improvement in overall efficiency.

The efficiency of the system has been enhanced through the optimization of the pilot plant, allowing for precise regulation of CO_2 injection and improved control over mesocosm preparation. Additionally, the deployment of better pumps and sensors has further increased experimental accuracy in assessing the targeted bicarbonate concentrations.

Fig. 4 shows the stability efficiency for each treatment over time. The stability efficiency in the S and H treatments with added DIC of 1992 and 1008 μmol C/L dropped below zero after almost 40 and 60 days, respectively. In contrast, L and M treatments with lower added alkalinity remained stable, maintaining efficiency above 90 % for nearly two months. Given that the saturation state of seawater in the S and H treatments was at or near the threshold for precipitation, this result highlights that higher alkalinity doses approaching this limit led to increased precipitation and inefficiency. The negative efficiency observed in the H and S treatments is in keeping with the DIC decline to levels below those of control seawater (Fig. 3), indicating a runaway precipitation phenomenon (Moras et al., 2022; Suitner et al., 2025) that caused continuous alkalinity loss. This behavior indicates that when alkalinity additions push the system into strongly supersaturated conditions, secondary precipitation may draw down not only the added

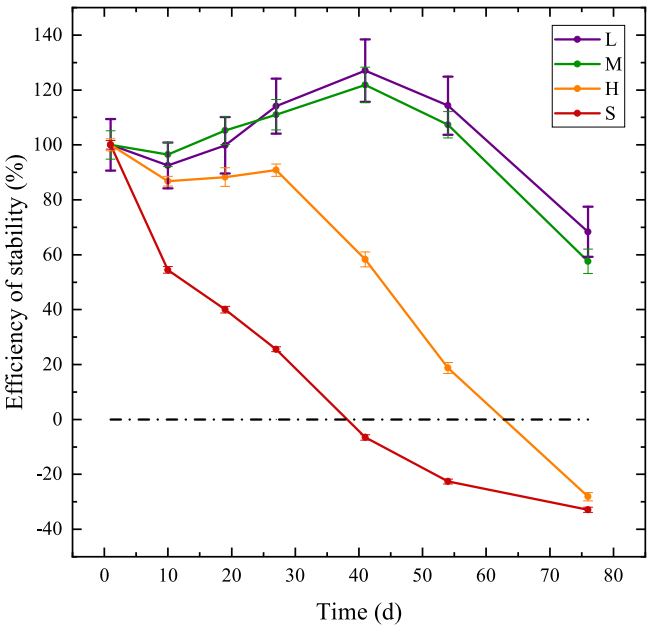

Fig. 4. Stability efficiency for each treatment over time. Error bars represent standard deviation across replicate mesocosms.

alkalinity but also part of the inherent seawater alkalinity, leading to an over-consumption of alkalinity. This over-consumption of natural alkalinity highlights an important implication for large-scale applications: when alkalinity additions approach highly supersaturated states, unintended alkalinity loss may occur, reducing net CO_2 retention efficiency. On the other hand, the greenhouse temperature oscillated from 15 °C in March to 36 °C in May (Fig. 3), contributing to the efficiency decline, particularly in the L and M treatments after almost two months. While temperature in the greenhouse went well above 30 °C, the actual atmospheric temperatures recorded in the sea at/around La Spezia have ranged from 11 to 28 °C over the past decade (Regione Liguria, 2025), with an average of 18 °C. The temperature rise during the experiment was not planned, but due to the closed environment of the greenhouse and to the warm spring conditions. The temperature values reached in the mesocosms are unrealistic for seawater, at least in this region. In fact, under real seawater conditions, where lower temperatures and plume spreading effect enhance solution dilution, stability is expected to improve, potentially allowing even higher added alkalinity levels without significant loss in efficiency. Recent findings also indicate that dilution below time-dependent critical thresholds of total alkalinity and Ω_{Ar} is essential to prevent net TA loss and ensure sustained stability (Suitner et al., 2024). This highlights the importance of incorporating dilution dynamics into both experimental design and large-scale application strategies.

It is interesting to assess whether the efficiency drop in the S and, with a delay, in the H treatments aligns with the supersaturation of minerals like aragonite. In these conditions, each bicarbonate addition intensifies supersaturation and, in extreme cases, induces secondary precipitation. As shown in Fig. 5, fluctuations in calculated average Ω_{Ar} occur even in the control treatment due to variations of ambient conditions within the greenhouse. To mitigate this effect, the relative Ω_{Ar}, namely the ratio of each treatment's Ω_{Ar} to the control, was calculated and is displayed in Fig. 5. This normalized curve confirms a sharp decline in Ω_{Ar} for the S treatment from the beginning of the experiment, indicating extensive nucleation and mineral precipitation. This is further corroborated by XRD analysis of collected precipitates, which confirms aragonite as the dominant mineral phase. A full breakdown of mineral abundances is presented in Table S1, and representative diffraction patterns are shown in Figure S2 (Supplementary materials). A similar

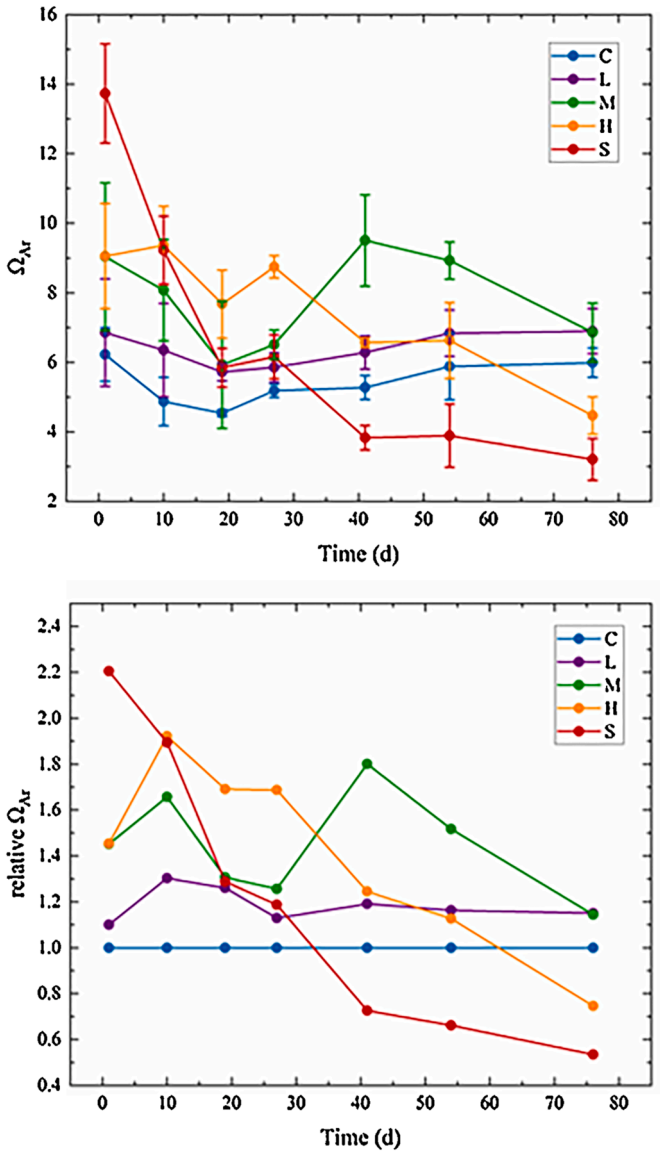

Fig. 5. Average Ω_{Ar} (top graph) and relative Ω_{Ar} (bottom graph) for each treatment over time. The calculation is based on the practical salinity of treatments from March to May 2024. Error bars represent standard deviation across replicate mesocosms.
Ω_{Ar} is the aragonite saturation state and relative Ω_{Ar} is defined as Ω_{Ar} (treatment)/Ω_{Ar} (control).

trend, albeit delayed, is observed in the H treatment.

As shown in Figure S3, in each treatment, including the control, some solid-state residual was eventually observed. The XRD analysis reveals that calcium carbonate is always present, in the form of aragonite and, to a much lesser extent, calcite (in combination with the Mg rich calcite, also known as magnesium calcite). The presence of NaCl (halite) is due to the filtering procedure, because the wet precipitates rapidly dry in air accumulating sodium chloride. Among the other precipitates, one finds also SiO_2 in the form of α-quartz and $CaSO_4$, in the form of gypsum ($CaSO_4{\cdot}2H_2O$). Aragonite is the dominant phase in H and S treatment, whereas Mg-rich calcite is more abundant in the control mesocosms and in one of the L treatment and M treatment mesocosms.

Notably, Fig. 5 shows that the control treatment's Ω_{Ar} on day 1 is significantly higher than the theoretical value reported in Table 1 (~3.4), with similar behavior observed for other treatments. Since theoretical calculations were based on seawater collected at the end of 2023, whereas the mesocosm experiment used seawater collected in March 2024, a broader investigation into the temporal variability of seawater characteristics in the Gulf of La Spezia was necessary. Fig. 6 reveals significant seasonal fluctuations in seawater salinity, particularly in shallower waters (Regione Liguria, 2025). Salinity tends to drop to ~34–35 PSU in March of each year, compared to ~38 PSU in December. This variation impacts the theoretical calculations. Therefore, it is crucial to consider the natural seawater characteristics such as salinity, pH, DIC, and temperature when determining the Ω_{Ar} threshold.

In Fig. 7, the Ω_{Ar} was calculated as a function of seawater salinity and temperature. Four scenarios were considered, representative of the C, L, M and S treatments. In addition, a contour line corresponding to $\Omega_{Ar} = 7$ has been added to each 2D map; this line is not intended as a stability threshold but rather serves as a visual reference to illustrate how supersaturation evolves across different seawater properties, including temperature and salinity. Because the C and L treatments do not reach Ω_{Ar} values comparable to those observed in the unstable H and S treatments ($\Omega_{Ar} > 10$), using a lower reference contour provides a consistent basis for comparing trends among treatments. The $\Omega_{Ar} = 7$ contour should therefore be regarded purely as a graphical guide to help visually identify conditions under which high alkalinity additions may lead to instability in the system. The pH values used for Ω_{Ar} calculations were seawater scale pH values derived from NIST scale pH, salinity, and temperature. The results indicate that, even at realistic seawater temperatures, high alkalinity dosages (S treatment) produce extremely high Ω_{Ar}, posing a very significant risk of carbonate precipitation. In contrast, the medium alkalinity addition (M treatment) allows for a wider range of seawater salinity and temperature without inducing a sharp increase in Ω_{Ar}. The Ω_{Ar} map for untreated seawater can serve as a baseline for future alkalinity regulation strategies.

This key finding underscores the influence of seasonal and climatic variations on seawater chemistry, highlighting the need to carefully consider the discharge location, operational season, and regional oceanographic conditions in large-scale application of ocean alkalinization (Ou et al., 2025; Zhou et al., 2025). According to Figs. 6 and 7, the alkalinity dosing should be continuously adjusted based on real-time local weather and seawater conditions. Implementing near-pH-equilibrated ocean alkalinization during stable periods, such as reduced rainfall or stable water circulation, may help maintain lower Ω_{Ar} even with substantial alkalinity additions, reducing the risk of secondary precipitation. Conversely, during months like March, when

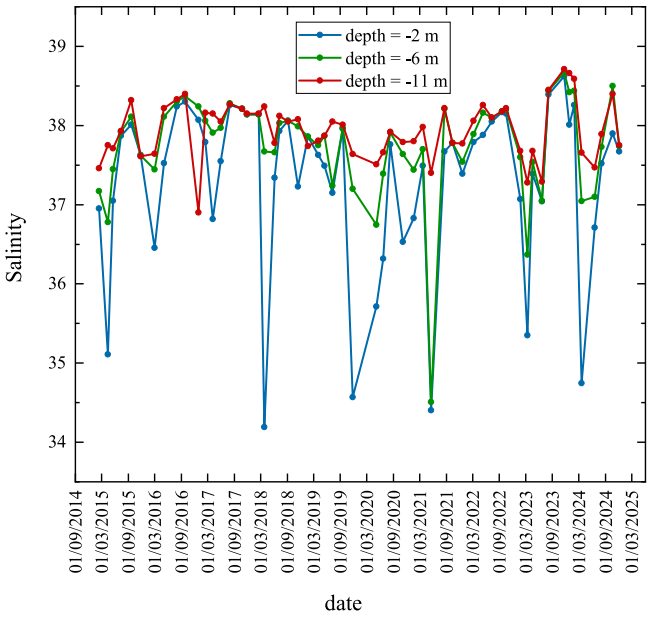

Fig. 6. Seawater Salinity in the Gulf of La Spezia records from 2015 to 2025. Salinity is expressed in practical salinity units (PSU).

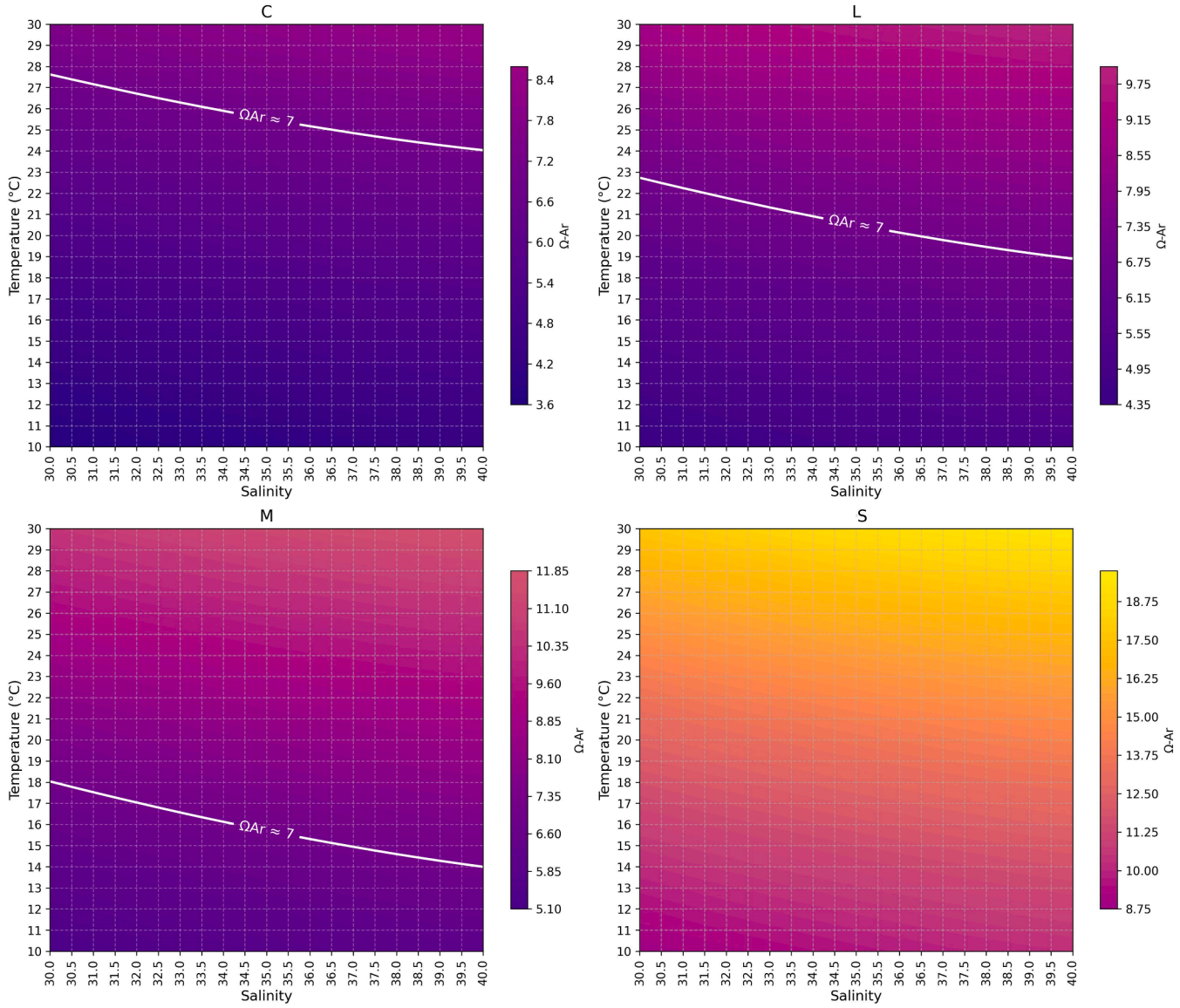

Fig. 7. 2D maps of Ω_{Ar} as a function of seawater salinity and temperature. C: Ω_{Ar} for control treatment at a constant seawater scale pH of 8.3. L: Ω_{Ar} for a representative L treatment (seawater scale pH = 8.34). M: Ω_{Ar} for a representative M treatment (seawater scale pH = 8.38). S: Ω_{Ar} for a representative S treatment (seawater scale pH = 8.44). A contour line corresponding to $\Omega_{Ar} = 7$ is included in each map. This line is not a stability threshold; rather, it is provided as a visual reference to illustrate how supersaturation patterns shift across changes in salinity and temperature and to enable consistent comparison among treatments. Ω_{Ar} is the aragonite saturation state. pH values used in the Ω_{Ar} calculations correspond to seawater scale pH derived from NIST scale measurements together with salinity and temperature.

salinity reaches its annual minimum, careful regulation of alkalinity input is necessary to prevent the supersaturation state of alkalinized seawater from exceeding the critical Ω_{Ar} threshold of 5, as recommended by Moras et al. (Moras et al., 2022). One important advantage of the near-pH-equilibrated ocean alkalinization is that it readily allows such a fine tuning of the added alkalinity, unlike, for example, the simple spreading of alkaline materials of the ocean surface.

4. Conclusions

Through this series of experiments, the process and the long-term efficiency of near-pH-equilibrated ocean alkalinization were investigated at a mesocosm scale in conditions very close to the real conditions for a Mediterranean site. These experiments demonstrate that the preparation and injection of a supersaturated solution ($\Omega_{Ar} > 10$) is inefficient and counterproductive. In fact, the process efficiency (preparation of the plume) is lower, and the treated seawater is not able to stabilize the high concentration of bicarbonate dissolved with almost immediate precipitation and degassing.

A medium concentration results in an efficient process which also features good long-term stability, provided the environmental temperature remains below $T = 30$ °C. Above that, precipitation and degassing are triggered. Only the medium and low concentrations remained stable for the entire duration of the long experiment, resisting to a temperature above 30 °C, although the medium concentration indicates potential instability if the high temperature is maintained for long period. This study therefore addresses which is undoubtedly the recommended concentration of bicarbonate in the plume that one should obtain to guarantee bicarbonate stability also under adverse conditions.

It should be noted that these experiments have tested two very unfavorable and unlikely situations: a) the seawater was collected in one of the periods of the year with lowest salinity (likely caused by several

rainy days before the operation); b) the temperature in the greenhouse remained significantly higher than the average outdoor temperature observed over an extended period throughout the year, reaching the highest temperatures of the site maintained for several days continuously (thus without night-time decreases). Both these situations adversely affect the pH-equilibrated ocean alkalinization.

For a correct application of the technique, one would therefore recommend tuning the concentration of the treatment depending on the atmosphere temperature of the seasons (therefore higher in winter and lower in summer) and the seawater salinity state that close to the coast vary as a function of fresh-water injection from rivers. These recommendations may therefore suggest the proper sites for the delivery of the treated seawater (for example far from the mouth of a river) and the seasonal load.

Funding

The experiments, whose results are presented in this paper, are funded by Limenet®, partly by a contract of Limenet ® with the Politecnico di Milano. The PhD grant of S.J.A., S. G. and D.C. is partly funded by MUR with a DM117 scholarship and partly funded by Limenet®.

Data availability

The deposited raw data are available at Zenodo: https://doi.org/10.5281/zenodo.15980848

CRediT authorship contribution statement

Samira Jamali Alamooti: Writing – review & editing, Writing – original draft, Methodology, Investigation, Formal analysis, Data curation, Conceptualization. **Federico Comazzi:** Investigation. **Eleonora Kratter Thaler:** Investigation. **Sara Groppelli:** Investigation. **Davide Calvi:** Investigation. **Guido Raos:** Writing – review & editing, Supervision, Methodology, Conceptualization. **Piero Macchi:** Writing – review & editing, Supervision, Methodology, Conceptualization.

Declaration of competing interest

The authors declare the following financial interests/personal relationships which may be considered as potential competing interests:

Piero Macchi reports financial support was provided by Limenet. Guido Raos reports financial support was provided by Limenet. Samira Jamali Alamooti reports financial support was provided by Limenet. Sara Groppelli reports financial support was provided by Limenet. Davide Calvi reports financial support was provided by Limenet. Federico Comazzi reports a relationship with Limenet that includes: employment. Liment owns the patent (PCT/IB2022/051464) of the process producing the marine bicarbonate solution analyzed in this study. If there are other authors, they declare that they have no known competing financial interests or personal relationships that could have appeared to influence the work reported in this paper.

Acknowledgments

The authors thank Porto Mirabello that hosted the experimental facility in La Spezia for the valuable support, and the Port Authority. F. C. thanks the accelerator Fund at CDP Venture Capital, for support.

Supplementary materials

Supplementary material associated with this article can be found, in the online version, at doi:10.1016/j.ijggc.2026.104589. It contains the full report of the XRD analysis and the diffraction patterns measured from each mesocosm is provided in the Supplementary materials.

References

Altomare, A., Corriero, N., Cuocci, C., Falcicchio, A., Moliterni, A., Rizzi, R., 2015. QUALX2.0: a qualitative phase analysis software using the freely available database POW-COD. J. Appl. Crystallogr. 48, 598–603. https://doi.org/10.1107/S1600576715002319.

Bach, L.T., Gill, S.J., Rickaby, R.E.M., Gore, S., Renforth, P., 2019. CO_2 removal with enhanced weathering and ocean alkalinity enhancement: potential risks and co-benefits for marine pelagic ecosystems. Front. Clim. 1, 7. https://doi.org/10.3389/fclim.2019.00007.

Badocco, D., Pedrini, F., Pastore, A., di Marco, V., Marin, M.G., Bogialli, S., Roverso, M., Pastore, P., 2021. Use of a simple empirical model for the accurate conversion of the seawater pH value measured with NIST calibration into seawater pH scales. Talanta 225, 122051. https://doi.org/10.1016/j.talanta.2020.122051.

Boyle, T.P., Fairchild, J.F., 1997. The role of mesocosm studies in ecological risk analysis. Ecol. Appl. 7, 1099–1102. https://doi.org/10.1890/1051-0761(1997)007[1099:TROMSI]2.0.CO;2.

Caldeira, K., Rau, G.H., 2000. Accelerating carbonate dissolution to sequester carbon dioxide in the ocean: geochemical implications. Geophys. Res. Lett. 27, 225–228. https://doi.org/10.1029/1999GL002364.

Campo, F., Caserini, S., Cappello, G., Righi, D., De Marco, S., Grosso, M., 2021. Buffered accelerated weathering of limestone as CO_2 storage technology: material and energy balance and cost analysis. In: SISC - Società Italiana per Le Scienze Del Clima 9th Annual Conference online.

Capelle, D.W., Kuzyk, Z.Z.A., Papakyriakou, T., Guéguen, C., Miller, L.A., Macdonald, R. W., 2020. Effect of terrestrial organic matter on ocean acidification and CO_2 flux in an Arctic shelf sea. Prog. Oceanogr. 185, 102319. https://doi.org/10.1016/j.pocean.2020.102319.

Caserini, S., Cappello, G., Righi, D., Raos, G., Campo, F., De Marco, S., Renforth, P., Varliero, S., Grosso, M., 2021. Buffered accelerated weathering of limestone for storing CO_2: chemical background. Int. J. Greenhouse Gas Control 112, 103517. https://doi.org/10.1016/j.ijggc.2021.103517.

Chou, W.C., Gong, G.C., Hsieh, P.S., Chang, M.H., Chen, H.Y., Yang, C.Y., Syu, R.W., 2015. Potential impacts of effluent from accelerated weathering of limestone on seawater carbon chemistry: a case study for the Hoping power plant in northeastern Taiwan. Mar. Chem. 168, 27–36. https://doi.org/10.1016/j.marchem.2014.10.008.

Coelho, A.A., 2018. TOPAS and TOPAS-Academic: an optimization program integrating computer algebra and crystallographic objects written in C^{++}. J. Appl. Crystallogr. 51, 210–218. https://doi.org/10.1107/S1600576718000183.

De Marco, S., Varliero, S., Caserini, S., Cappello, G., Raos, G., Campo, F., Grosso, M., 2023. Techno-economic evaluation of buffered accelerated weathering of limestone as a CO_2 capture and storage option. Mitig. Adapt. Strateg. Glob. Change 28, 17. https://doi.org/10.1007/s11027-023-10052-x.

Dickson, A.G., Millero, F.J., 1987. A comparison of the equilibrium constants for the dissociation of carbonic acid in seawater media. Deep Sea Res. Part A. Oceanogr. Res. Papers 34, 1733–1743. https://doi.org/10.1016/0198-0149(87)90021-5.

Dickson, A., 1990. Standard potential of the reaction: $AgCl(s) + 1/2\ H_2(g) = Ag\ (s) + HCl\ (aq)$, and the standard acidity constant of the ion HSO_4^- in synthetic sea water from 273.15 to 318.15 K. J. Chem. Thermodyn. 22, 113–127. https://doi.org/10.1016/0021-9614(90)90074-Z.

Falini, G., Fermani, S., Gazzano, M., Ripamonti, A., 1998. Materials structure and morphology of synthetic magnesium calcite. J. Mater. Chem. 8, 1061–1065. https://doi.org/10.1039/A707893E.

Groppelli, S., Calvi, D., Comazzi, F., Azzellino, A., Jamali Alamooti, S., Macchi, P., Raos, G., Barbaccia, E., Caronni, S., Basso, D., 2026. The response of Phytoplankton to pH-equilibrated ocean alkalinization: a Mesocosm experiment with harbour water. Mar. Pollut. Bull. 222 (Part 2), 118787. https://doi.org/10.1016/j.marpolbul.2025.118787.

Hartmann, J., West, A.J., Renforth, P., Köhler, P., De La Rocha, C.L., Wolf-Gladrow, D.A., Dürr, H.H., Scheffran, J., 2013. Enhanced chemical weathering as a geoengineering strategy to reduce atmospheric carbon dioxide, supply nutrients, and mitigate ocean acidification. Rev. Geophys. 51, 113–149. https://doi.org/10.1002/rog.20004.

Hartmann, J., Suitner, N., Lim, C., Schneider, J., Marín-Samper, L., Arístegui, J., Renforth, P., Taucher, J., Riebesell, U., 2023. Stability of alkalinity in ocean alkalinity enhancement (OAE) approaches - consequences for durability of CO_2 storage. Biogeosciences. 20, 781–802. https://doi.org/10.5194/bg-20-781-2023.

Huysmans, T., Meysman, F.J.R., van de Velde, S.J., 2025. Reviews and syntheses: potential and limitations of oceanic carbon dioxide storage via reactor-based accelerated weathering of limestone. Biogeosciences. 22, 5557–5572. https://doi.org/10.5194/bg-22-5557-2025.

Ilyina, T., Wolf-Gladrow, D., Munhoven, G., Heinze, C., 2013. Assessing the potential of calcium-based artificial ocean alkalinization to mitigate rising atmospheric CO_2 and ocean acidification. Geophys. Res. Lett. 40, 5909–5914. https://doi.org/10.1002/2013GL057981.

Intergovernmental Panel on Climate Change (IPCC), 2005. Special report: carbon dioxide capture and storage.

Intergovernmental Panel on Climate Change (IPCC), 2023. Climate Change 2021 – The physical Science Basis Summary For policymakers, Climate Change 2021 – The Physical Science Basis. Cambridge University Press. https://doi.org/10.1017/9781009157896.001.

Köhler, P., 2020. Anthropogenic CO_2 of high emission scenario compensated after 3500 years of ocean alkalinization with an annually constant dissolution of 5 pg of Olivine. Front. Clim. 2, 575744. https://doi.org/10.3389/fclim.2020.575744.

Kheshgi, H.S., 1995. Sequestering atmospheric carbon dioxide by increasing ocean alkalinity. Energy 20, 915–922. https://doi.org/10.1016/0360-5442(95)00035-F.

Kirchner, J.S., Berry, A., Ohnemüller, F., Schnetger, B., Erich, E., Brumsack, H.J., Lettmann, K.A., 2020a. Reducing CO_2 emissions of a coal-fired power plant via accelerated weathering of limestone: carbon capture efficiency and environmental safety. Environ. Sci. Technol. 54, 4528–4535. https://doi.org/10.1021/acs.est.9b07009.

Kirchner, J.S., Lettmann, K.A., Schnetger, B., Wolff, J.O., Brumsack, H.J., 2020b. Carbon capture via accelerated weathering of limestone: modeling local impacts on the carbonate chemistry of the southern North Sea. Int. J. Greenhouse Gas Control 92, 102855. https://doi.org/10.1016/j.ijggc.2019.102855.

Lewis, E.L., 1980. The practical salinity scale 1978 and its antecedents. IEEE J. Oceanic Eng. OE 5, 3–8. https://doi.org/10.1109/joe.1980.1145448.

Mehrbach, C., Culberson, C.H., Hawley, J.E., Pytkowicx, R.M., 1973. Measurement of the apparent dissociation constants of carbonic acid in seawater at atmospheric pressure. Limnol. Oceanogr. 18, 897–907. https://doi.org/10.4319/lo.1973.18.6.0897.

Moras, C.A., Bach, L.T., Cyronak, T., Joannes-Boyau, R., Schulz, K.G., 2022. Ocean alkalinity enhancement - avoiding runaway $CaCO_3$ precipitation during quick and hydrated lime dissolution. Biogeosciences. 19, 3537–3557. https://doi.org/10.5194/bg-19-3537-2022.

National Academies of Sciences, Engineering and Medicine, 2022. A Research Strategy For Ocean-Based Carbon Dioxide Removal and sequestration, A Research Strategy for Ocean-based Carbon Dioxide Removal and Sequestration. National Academies Press. https://doi.org/10.17226/26278.

Ou, Y., Xue, Z.G., Hu, X., 2025. A numerical assessment of ocean alkalinity enhancement efficiency on a river-dominated continental shelf—A case study in the northern Gulf of Mexico. Environ. Res. Lett. 20, 024031. https://doi.org/10.1088/1748-9326/adaa8b.

Pierrot, D., Lewis, E., Wallace, D., 2006. MS Excel program developed for CO2 system calculations. https://doi.org/10.3334/CDIAC/otg.CO2SYS_XLS_CDIAC105a.

Rau, G.H., Caldeira, K., 1999. Enhanced carbonate dissolution: a means of sequestering waste CO_2 as ocean bicarbonate. Energy Convers. Manage. 40, 1803–1813. https://doi.org/10.1016/S0196-8904(99)00071-0.

Rau, G.H., 2011. CO_2 mitigation via capture and chemical conversion in seawater. Environ. Sci. Technol. 45, 1088–1092. https://doi.org/10.1021/es102671x.

Regione Liguria, 2025. Qualità delle acque marine. Regione Liguria, Genova, Italy. URL https://servizi.regione.liguria.it/page/welcome/QUALITA_ACQUE_MARINE (accessed 4.13.25).

Renforth, P., Baltruschat, S., Peterson, K., Mihailova, B.D., Hartmann, J., 2022. Using ikaite and other hydrated carbonate minerals to increase ocean alkalinity for carbon dioxide removal and environmental remediation. Joule 6, 2674–2679. https://doi.org/10.1016/j.joule.2022.11.001.

Ringham, M.C., Hirtle, N., Shaw, C., Lu, X., Herndon, J., Carter, B.R., Eisaman, M.D., 2024. An assessment of ocean alkalinity enhancement using aqueous hydroxides: kinetics, efficiency, and precipitation thresholds. Biogeosciences. 21, 3551–3570. https://doi.org/10.5194/bg-21-3551-2024.

Sánchez, N., U Goldenberg, S., Brüggemann, D., Jaspers, C., Taucher, J., Riebesell, U., 2024. Plankton food web structure and productivity under ocean alkalinity enhancement. Sci. Adv. 10, eado0264. https://doi.org/10.1126/sciadv.ado0264.

Suitner, N., Faucher, G., Lim, C., Schneider, J., Moras, C.A., Riebesell, U., Hartmann, J., 2024. Ocean alkalinity enhancement approaches and the predictability of runaway precipitation processes: results of an experimental study to determine critical alkalinity ranges for safe and sustainable application scenarios. Biogeosciences. 21, 4587–4604. https://doi.org/10.5194/bg-21-4587-2024.

Suitner, N., Hartmann, J., Varliero, S., Faucher, G., Suessle, P., Moras, C.A., 2025. Surface area and Ω-aragonite oversaturation as controls of the runaway precipitation process in ocean alkalinity enhancement. EGUsphere. https://doi.org/10.5194/egusphere-2025-381 [preprint].

Taylor, L.L., Quirk, J., Thorley, R.M.S., Kharecha, P.A., Hansen, J., Ridgwell, A., Lomas, M.R., Banwart, S.A., Beerling, D.J., 2016. Enhanced weathering strategies for stabilizing climate and averting ocean acidification. Nat. Clim. Change 6, 402–406. https://doi.org/10.1038/nclimate2882.

Uppstrom, L.R., 1974. The boron/chlorinity ratio of deep-sea water from the Pacific Ocean. Deep-Sea Res. 21, 161–162. https://doi.org/10.1016/0011-7471(74)90074-6.

Varliero, S., Alamooti, S.J., Campo, F.Pietro, Cappello, G., Cappello, S., Caserini, S., Comazzi, F., Macchi, P., Raos, G., 2024. Assessing the limit of CO_2 storage in seawater as bicarbonate-enriched solutions. Molecules. 29, 4069. https://doi.org/10.3390/molecules29174069.

Varliero, S., 2021. Modelling of Calcite and Dolomite Dissolution in the Buffered Accelerated Weathering of Limestone Technology For CO_2 Storage (MSc Thesis). Politecnico di Milano, Milan, Italy.

Vibbert, H.B., Park, A.H.A., 2022. Harvesting, storing, and converting carbon from the ocean to create a new carbon economy: challenges and opportunities. Front. Energy Res. 10, 999307. https://doi.org/10.3389/fenrg.2022.999307.

Xin, X., Urs Goldenberg, S., Taucher, J., Stuhr, A., Arístegui, J., Riebesell, U., 2024. Resilience of phytoplankton and microzooplankton communities under ocean alkalinity enhancement in the oligotrophic ocean. Environ. Sci. Technol. 58, 20918–20930. https://doi.org/10.1021/acs.est.4c09838.

Zeebe, R.E., Wolf-Gladrow, D., 2001. CO_2 in Seawater: Equilibrium, kinetics, Isotopes, 1st ed. Elsevier Science.

Zhou, M., Tyka, M.D., Ho, D.T., Yankovsky, E., Bachman, S., Nicholas, T., Karspeck, A.R., Long, M.C., 2025. Mapping the global variation in the efficiency of ocean alkalinity enhancement for carbon dioxide removal. Nat. Clim. Change 15, 59–65. https://doi.org/10.1038/s41558-024-02179-9.

Zhuang, W., Song, X., Liu, M., Wang, Q., Song, J., Duan, L., Li, X., Yuan, H., 2023. Potential capture and conversion of CO_2 from oceanwater through mineral carbonation. Sci. Total. Environ. 867, 161589. https://doi.org/10.1016/j.scitotenv.2023.161589.